SPE-199958-MS

The Effect of Solvent based Nanofluid Flooding on Heavy Oil Recovery

Sepideh Maaref, Department of Chemical and Petroleum Engineering, University of Calgary, Calgary, AB, Canada; Apostolos Kantzas, Department of Chemical and Petroleum Engineering, University of Calgary, Calgary, AB, Canada, PERM Inc. TIPM Laboratory, Calgary, AB, Canada; Steven L. Bryant, Department of Chemical and Petroleum Engineering, University of Calgary, Calgary, AB, Canada, Canada Excellence Research Chair in Materials Engineering for Unconventional Oil Reservoirs, Canada

This paper was prepared for presentation at the SPE Canada Heavy Oil Techncial Conference originally scheduled to be held in Calgary, Alberta, Canada, 18 – 19 March 2020. Due to COVID-19 the physical event was postponed until 29 September – 2 October 2020 and was changed to a virtual event. The official proceedings were published online on 24 September 2020.

Abstract

The objective of this study is to investigate the effect of solvent based nanofluid flooding followed by waterflooding on heavy oil recovery performance and sweep efficiency improvement in unconsolidated oil-wet porous media. The sweep efficiency improvement is correlated with in-situ emulsion generation during such displacement and is monitored with a CT scanner.

Partially hydrophobic silica NPs with proper interface affinity was firstly synthesized, and subsequently dispersed in toluene along with a surfactant to prepare the solvent based nanofluid. The solvent based nanofluid was then injected into an oil saturated sandpack at different slug sizes and further chased by brine to investigate the sweep efficiency improvement through possible emulsification. To investigate the beneficial effect of NPs, the aforementioned flooding was compared against conventional solvent flooding followed by waterflooding. The displacement patterns were monitored with a CT-scanner to assess the heavy oil recovery performance in the absence or presence of the solvent based nanofluid.

The fluid density profiles during solvent based NF flooding followed by waterflooding were extracted from CT-scan images and compared against conventional solvent flooding followed by waterflooding to assess potential sweep efficiency improvement. The results revealed an increase in sweep efficiency during solvent based NF flooding followed by waterflooding. This was related to the creation of in-situ emulsion at the water-diluted oil interface due to the presence of NPs and surfactant in diluted oil. Unlike conventional solvent flooding where post water created several fingers through porous media, the water phase in solvent based nanofluid flooding was able to displace all the lower resistance paths created by the solvent based nanofluid. Moreover, chase water was able to recover almost all of the solvent in solvent based NF flooding, which is essential for the process to be economically viable. In general, the presence of solvent based NF was found to be effective in re- distributing the preferential water flow paths in to a more uniform front, which suppressed the fingering in turn and resulted in later water breakthrough, better sweep efficiency, and higher oil recovery.

The proposed solvent based nanofluid flooding has not been tested so far as a heavy oil recovery technique. Unlike conventional solvent flooding which can suffer from high residual solvent to waterflooding, this technique revealed negligible residual solvent upon waterflooding. Moreover, it was found to be effective in sweep efficiency improvement and heavy oil recovery compared to conventional solvent flooding.

INTRODUCTION

The key problem in heavy oil reservoirs is inefficient sweep due to the low mobility of the oil [1]. With the primary production, around only 5 % of the heavy oil in place could be recovered [2] and waterflooding, as the most commonly used and economically viable form of secondary recovery, could merely produce another 5 to 10% of the heavy oil in place [3–4]. This is because a large proportion of oil is bypassed due to viscous fingers caused by the adverse mobility ratio between the viscous oil and water. The most commonly used techniques to improve the recovery of heavy oil are aimed to reduce the oil viscosity by using steam or solvents [2].

Although thermal methods including steam flooding, cyclic steam stimulation (CSS), SAGD and in-situ combustion have been applied as the most effective techniques to recover heavy oil by oil viscosity reduction as well as oil production by gravity and viscous displacements [5], their application to deep or thin heavy oil reservoirs is economically unfeasible due to heat losses to overburden, underburden, and aquifer [6]. Furthermore, high energy consumption, CO_2 emission, fresh water source requirements for steam generation, and waste water treatment has attracted more attention to the use of non-thermal methods to enhance heavy oil recovery [5].

Solvent flooding is one of the non-thermal methods which is aimed to develop miscibility with the oil phase to mobilize the residual oil and enhance the mobility of hydrocarbon phase by oil viscosity reduction [7–9]. Several solvents including aromatic hydrocarbons such as toluene, benzene, and xylene as well as paraffinic hydrocarbons such as propane, butane, pentane, hexane, etc. can be dissolved in heavy oil [10]. However, solvent injection is cost sensitive [7, 11] and requires an optimization by maximizing the solvent retrieval and optimizing the amount injected [7]. Due to the cost of miscible solvents, slug processes are generally used. The required slug size is affected by several parameters such as reservoir heterogeneity, well spacing, gravity effects, mobility ratios, etc. [12].

In heavy oil reservoirs, solvent injection can be conducted solely in the form of vapor extraction (VAPEX) [13] or cyclic solvent injection (CSI) or can be applied in combination with a thermal method [7]. The use of solvent with thermal methods to further reduce the oil viscosity has been considered widely in the form of LASER (liquid addition to steam to enhance recovery) or other hybrid steam-solvent processes such as ES-SAGD [14]. There are also several studies which tested solvent co-injection with steam, pre-injection of solvent prior to steam injection processes [15–20], or solvent alternating steam injection [14, 21]. In such processes, solvent dissolves to the oil to decrease oil viscosity and enhance the oil mobility in the vicinity of steam chamber boundary [22–23]. Therefore, the combined effect of heat transfer and dilution in steam-based solvent processes for heavy oil recovery yields a better result than the application of steam or cold solvent alone [13, 24–32].

For reservoirs with not extremely heavy oil (or bitumen), solvent injection can be done solely in homogeneous [33] and heterogeneous reservoirs [7, 34–37]. Although solvent injection in such reservoirs results in high local displacement efficiency, the overall efficiency of the process can be compromised by viscous fingering, channeling, and gravity override [8, 38–39]. One method to overcome the poor mobility ratio is to conduct water alternating solvent (WAS) injection [7–8, 40]. This process has been also found to be effective in solvent retrieval due to the presence of water slugs, which make the process economically viable [7, 40].

There are also some studies that reported the use of emulsified solvent flooding (s/w emulsion) as an alternative to miscible solvent injection [41–42]. The idea is very similar to that of o/w emulsion flooding for

improving the waterflood performance and controlling the mobility [41]. There are some advantages with this process including higher displacement efficiency with lower cost due to the reduced solvent requirement. Moreover, emulsified solvent flooding would be less prone to viscous fingering compared to miscible solvent flooding, resulting in sweep efficiency improvement [41]. The mechanisms responsible for heavy oil recovery by emulsified solvent flooding has been mentioned to be mobility control, oil viscosity reduction, IFT reduction, and in-situ emulsification of oil, among which the mobility reduction by trapping of emulsion droplets as well as oil viscosity reduction has appeared to be dominant mechanisms [41].

Based on solvent injection studies in both conventional and heavy oil reservoirs, the oil recovery as well as solvent retrieval are essential for the process to be technically and economically feasible [7]. The objective of this study is to satisfy these two criteria by the application of solvent based nanofluid flooding followed by waterflooding as a mobility control technique, which has not been tested so far in literature. In addition to the oil viscosity reduction due to the presence of solvent, the presence of nanoparticles and a co-stabilizing surfactant in solvent based nanofluid is able to generate in-situ emulsion with the chase water. This process is both technically and economically viable as in-situ emulsion generation would result in sweep efficiency improvement and the presence of chase water is effective in solvent retrieval. The sweep efficiency improvement during solvent based nanofluid flooding followed by waterflooding is derived from real time monitoring of fluid density profiles using a computed tomography (CT) scanner and solvent retrieval is calculated based on the effluent sample analysis.

MATERIALS AND METHODS

Test Fluids

Hydrophilic silica nanoparticles were firstly synthesized in this study as the most commonly used and cost-effective option for oil recovery applications. They were subsequently treated with a chemical reagent, hexamethyldisilazane (HMDS), to become partially hydrophobic [43]. Several characterization tests were conducted on both hydrophilic and partially hydrophobic silica NPs to assess the efficiency of modification, which are mentioned in detail in our previously published work [43]. Based on the characterization tests, the size of partially hydrophobic silica NPs (HSNP) was measured to be 137.2 nm with a reduction of 49% in surface hydroxyl group of the particles after modification. Due to the presence of both hydroxyl groups (Si-OH) and hydrocarbon groups (trimethylsiloxy (Si-O-Si-$(CH_3)_3$) on the surface of HSNP, they revealed proper affinity to the interface of oil and water phases as well as the ability to be dispersed in the hydrocarbon phase.

To prepare a solvent based nanofluid, 0.5 %wt. of partially hydrophobic silica NPs (HSNP) with 0.5 %wt. of a co-stabilizing surfactant (Span® 80) were dispersed in toluene. Toluene was used as a solvent in this study to prevent possible asphaltene precipitation with the oil phase. A Western Canada heavy oil sample provided by CNRL was used as the oil phase in this study, which was diluted with 20% toluene by volume to reach a viscosity of 100 mPas for all experiments. The brine phase used for waterflooding was 1 %wt. potassium iodide (KI) in deionized water to provide contrast for CT scanning. The properties of the fluids used in the core flooding experiments are mentioned in Table 1.

Table 1—The test fluids properties used in the core flooding experiments.

Test	T1: Control	T2: S/0.1 PV	T3: SNF/0.1 PV	T4: S/1 PV	T5: SNF/1 PV
Solvent type/Slug size	N/A	Toluene/0.1 PV	Toluene with NPs and surfactant/0.1 PV	Toluene/1PV	Toluene with NPs and surfactant/1 PV
Brine	1 %wt. KI	1 %wt. KI	1 %wt. KI	1 %wt. KI	1 %wt. KI
NP type	N/A	N/A	HSNP	N/A	HSNP
NP Conc. (%wt.)	0	0	0.5	0	0.5
Surfactant type	N/A	N/A	Span® 80	N/A	Span® 80
Surfactant conc. (%wt.)	0	0	0.5	0	0.5
ρ_w(kg/m^3)	1006.1	1006.1	1004.3	1005.9	1006.1
ρ_o(kg/m^3)	940.2	943.8	943.8	941.4	943.8
ρ_s(kg/m^3)	N/A	866.9	871.6	866.9	871.6
μ_w(mPas)	1.12	1.12	1.12	1.12	1.12
μ_o(mPas)	100.15	102.67	102.67	101.27	103.17
μ_s(mPas)	N/A	0.54	0.69	0.54	0.69

* ρ_s and μ_s are the solvent density and viscosity.

* S and SNF are the solvent and solvent based nanofluid.

Core flooding Experiments

A series of core flooding experiments were designed in an oil-wet sandpack to assess the effect of solvent based nanofluid flooding followed by waterflooding on sweep efficiency and oil recovery. The schematic of the core flooding set-up is shown in Figure 1, consisting of: a sandpack which is embedded in a CT-scanner, an Isco syringe pump to inject fluids, transfer vessels, a pressure transducer, and a data acquisition system which is integrated to a processing software. The sandpack used in this study is 31 cm long with an internal diameter of 2.54 cm. The sand particles were 50-70 mesh particle sizes which were treated with SurfaSil™ siliconizing fluid to become oil-wet. Table 2 presents the physical and hydraulic properties of the sandpack used in each experiment.

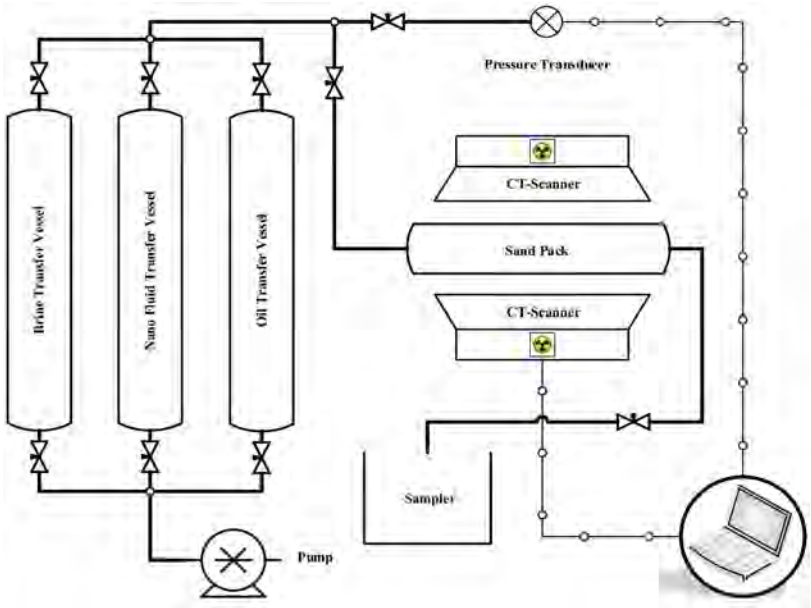

Figure 1—Schematic of the core flooding set-up embedded in a CT-scanner.

Table 2—Physical and hydraulic properties of sandpack.

Test	T1: Control	T2: S/0.1 PV	T3: SNF/ 0.1 PV	T4: S/1 PV	T5: SNF/1 PV
φ (%)	37.7	38.2	38.3	38.4	37.8
K (d)	25.14	24.9	26.1	25.8	24.3
PV (cm^3)	59.3	60.03	60.19	60.29	59.43
S_{oi}	0.89	0.87	0.88	0.89	0.88
S_{wi}	0.11	0.13	0.12	0.11	0.12
Q (cm^3/min)	0.5	0.5	0.5	0.5	0.5
V (ft/day)	4.66	4.66	4.66	4.66	4.66

Prior to any experiment, the sandpack was vacuumed and fully saturated with deionized water. Afterwards, crude oil was injected at a constant flow rate of 3 cm^3/min for two pore volumes to saturate the sandpack with oil in the presence of connate water saturation. Figure 2 illustrates the schematic of the core flooding experiments conducted in the oil saturated sandpacks in tests T1 to T5.

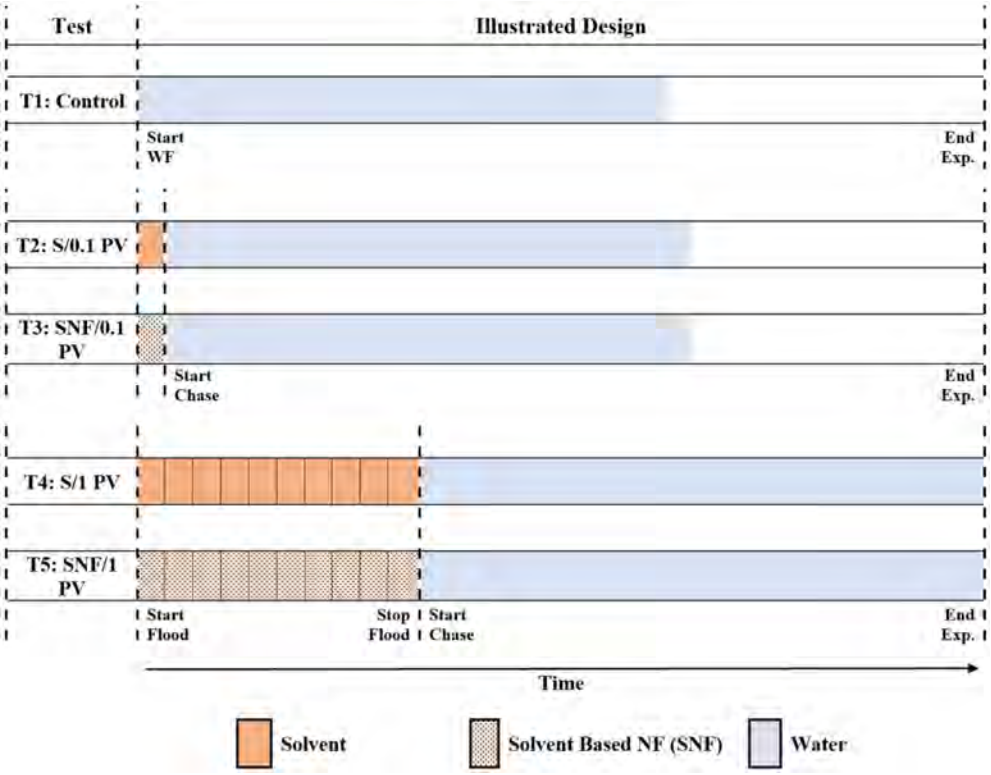

Figure 2—An illustration of core flooding experiments conducted in tests T1 to T5. WF, S, and SNF denote waterflooding, solvent, and solvent based nanofluid, respectively.

According to Figure 2, a control experiment (T1) was firstly conducted by injecting brine (waterflooding) at a constant injection rate of 0.5 cm^3/min for 2.5 pore volumes. Conventional solvent flooding was conducted in experiment T2 as a baseline. In test T2, toluene was injected into the oil saturated sandpack at a constant flow rate of 0.5 cm^3/min and a slug size of 0.1 pore volume (PV). Waterflooding was conducted afterwards at a constant flow rate of 0.5 cm^3/min for 2.5 pore volumes to displace the solvent.

To conduct solvent based nanofluid flooding and compare it against conventional solvent flooding, test T3 was conducted in the presence of NPs and surfactant (see Figure 2). In test T3, toluene with 0.5 %wt. HSNP and 0.5 %wt. Span® 80 was injected into the oil saturated sandpack at a rate of 0.5 cm^3/min and a

slug size of 0.1 PV. It was then followed by 2.5 pore volumes of brine at 0.5 cm^3/min to assess potential sweep efficiency improvement through in-situ emulsification in the presence of the solvent based nanofluid.

To investigate the effect of solvent slug size, tests T4 and T5 were conducted similar to that of tests T2 and T3 at a slug size of 1 pore volume (see Figure 2). In test T4, 1 pore volume of toluene in the absence of NPs and surfactant was injected into the oil saturated sandpack, followed by 2.5 pore volumes of brine at a constant flow rate of 0.5 cm^3/min. Test T4 was then compared against test T5 in which 1 pore volume of solvent based nanofluid (toluene with HSNP and Span® 80) was injected into the oil saturated sandpack and was further followed by 2.5 pore volumes of brine. It should be noted that a test in the presence of surfactant alone (0.5 %wt. Span® 80) in the solvent phase was also conducted in our previous research using a mineral oil [44]. However, it was found that the presence of NPs and surfactant was more effective than the presence of surfactant alone as they were able to enhance the oil production rate with much lower pressure drawdown compared to the surfactant alone test [44]. That is why the tests with both NPs and surfactant were only conducted for the crude oil experiments.

The internal displacement dynamics during waterflooding of tests T1 to T5 were monitored in real time using a medical CT-scanner. The scanning was conducted every 1 cm along the sandpack at different pore volumes of brine injection and several standard samples were scanned along the sandpack for calibration. Fluid density profiles during waterflooding of tests T1 to T5 was obtained by processing CT scan images at different pore volumes of brine injection. The obtained density profiles were subsequently compared with each other to assess potential sweep efficiency improvement during solvent based nanofluid flooding.

Effluent Sample Analysis

To evaluate solvent retrieval and oil recovery performance, effluent samples were analyzed in several steps. The mass of each effluent vial was measured before and after sampling. After sampling, the effluent samples were centrifuged at 4000 RPM for 30 minutes to separate the oil and water phases. The volume of water phase was then recorded and corrected according to the previously measured masses. Using a separator funnel, the water phase was discharged from the mixture of oil and toluene (solvent). The mixture of oil and toluene was then transferred to a rotary evaporator apparatus to evaporate the toluene at 70 ˚C and 125 mbar, leaving the oil phase behind. It should be mentioned that the amount of the oil phase loss during evaporation at 70 ˚C and 125 mbar was measured separately with an oil sample and found to be negligible. Since the oil phase loss was negligible, the mass of the oil phase remained after evaporating toluene was measured and converted to the oil volume using the oil density. It should be noted that since the oil phase was diluted with 20% toluene by volume, the oil volume was corrected accordingly. The solvent (toluene) mass was calculated by subtracting the total fluid mass of each vial from the water phase and diluted oil phase masses. The solvent mass was subsequently converted to the solvent volume using the solvent (toluene) density. This procedure was repeated for all effluent vials to obtain the oil and solvent recovery as a function of the pore volume injected.

RESULTS AND DISCUSSION

This section starts with comparing the fluid density profiles obtained from processing CT scans for tests T1 to T5. Afterwards, the oil and solvent recovery, IFT and contact angle measurements as well as pressure drop performance are presented for tests T1 to T5. The obtained results are compared against each other to investigate the effect of solvent based nanofluid flooding followed by waterflooding on sweep efficiency, oil recovery, and solvent retrieval performance.

Fluid Density Profiles

T1: Control Experiment. Figure 3 and Figure 4 show the fluid density profiles obtained from processing CT scan images at different pore volumes of brine injection into an oil saturated sandpack for the control

experiment (T1). The blue regions in Figure 4 represent the water phase density and red regions represent the oil phase density. Moreover, the density values reported here are apparent density values to accommodate for the enhanced CT contrast using potassium iodide. The lateral CT images during waterflooding of test T1 are shown at two different planes of x-z and y-z in Figure 4 (a) and Figure 4 (b), respectively. Figure 4 (c) also shows the cross-sectional CT slices as well as the sandpack 3D visualization at 0.18 pore volume of brine injection (PVI). According to the 3D reconstruction image in Figure 4 (c), x-z plane represent the sandpack view from top (horizontally) and y-z plane represent the sandpack view from the side (vertically), with gravity pointing downward. IC represents the initial condition of the sandpack: saturated with the oil phase with connate water saturation, hence the uniform density profile in Figure 3 and uniform red regions in Figure 4.

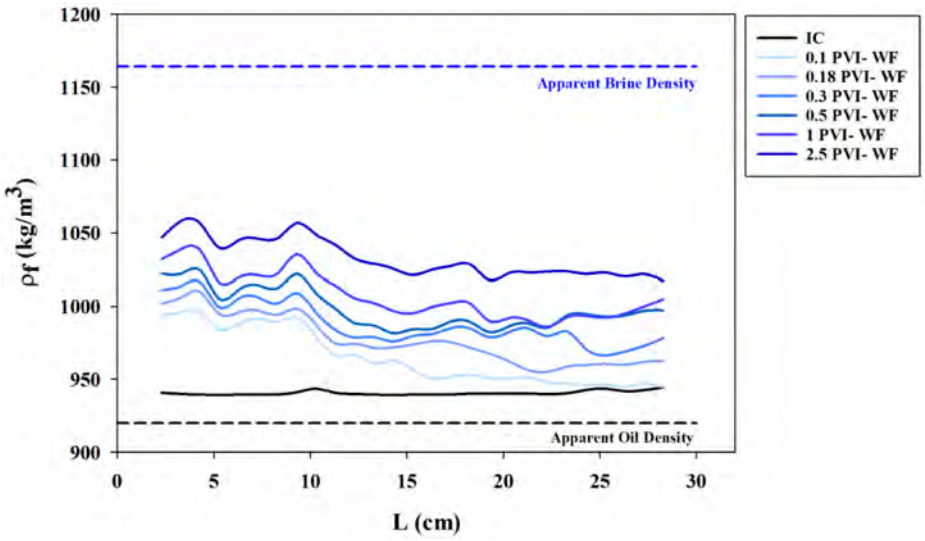

Figure 3—Fluid density profiles along the sandpack for test T1: Control at different pore volumes of water injection. IC (black) is the initial condition (oil and water at connate water saturation). WF denotes waterflooding. Light to dark blue are profiles for waterflooding as PVI increases.

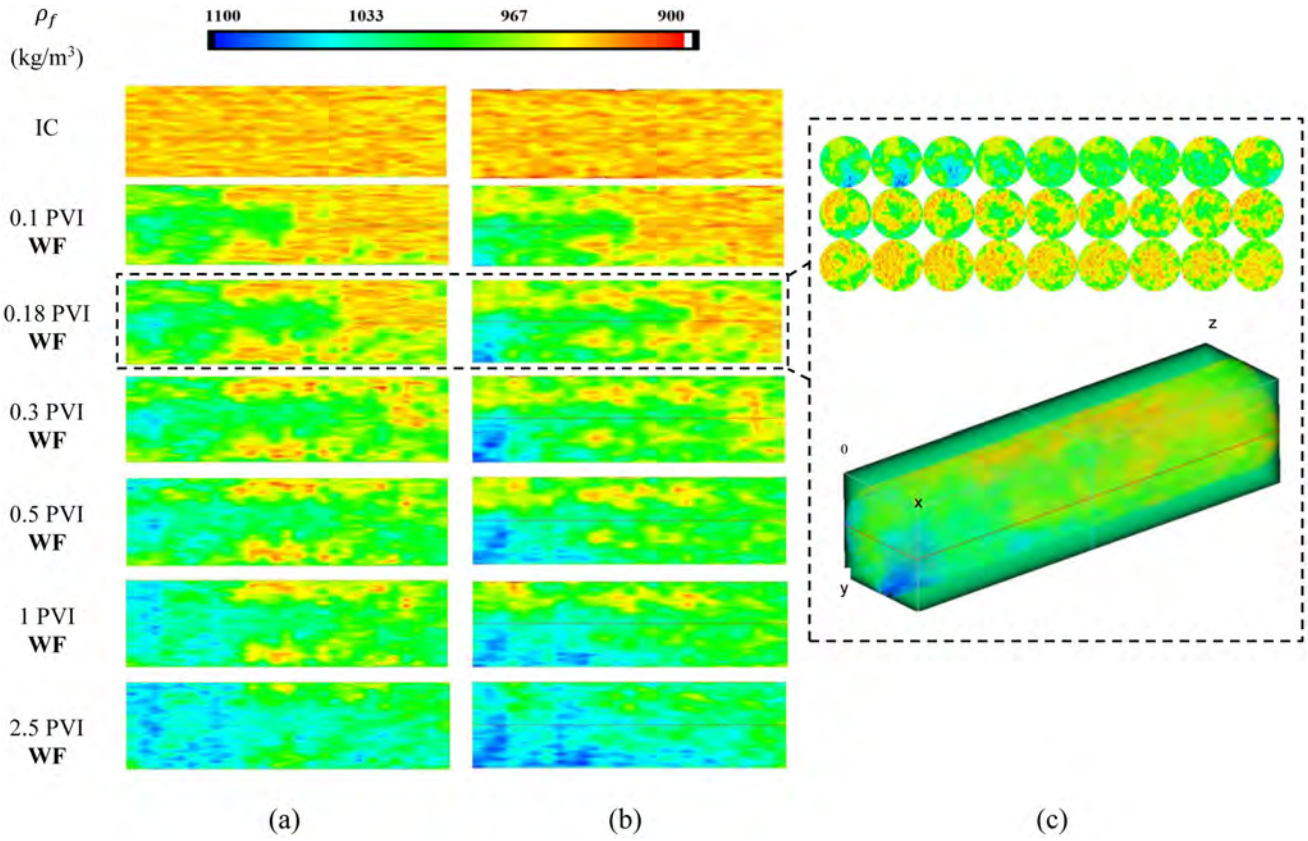

Figure 4—Lateral CT scans during waterflooding of test T1 (control experiment) at two different planes of (a) x-z and (b) y-z. WF denotes waterflooding. (c) Cross sectional CT slices of test T1: control at 0.18 PVI (top) and the corresponding 3D reconstruction view (bottom).

According to Figure 3 and Figure 4, the displacement front is not uniform during waterflooding of heavy oil (T1). As can be found specially in the vertical view (y-z plane) in Figure 4, there are high water saturation regions (blue) next to the regions of high oil saturation (red). This represent the non-uniform displacement of the injected brine as a result of the unfavorable mobility ratio between the oil and water phases. Moreover, there are some signs of gravity underride of the water phase, especially after 0.3 PVI in the y-z direction. This is due to the tendency of the water phase to displace the medium in a gravity stable manner as it has higher density than the oil phase (see Table 1). By careful examination of Figure 4 (b) at late pore volumes of brine injection, it is clear that some of the oil phases are bypassed by the brine phase due to the viscous fingering effect and the main part of the oil phase are trapped in the upper regions of the sandpack as a result of the water gravity underride. The control experiment (T1) shown here has clearly addressed both the fingered flow and gravitational segregation in an adverse mobility ratio condition and has been used as a base line to further investigate the effect of presenting solvent or solvent based nanofluid on displacement dynamics.

T2: S/0.1 PV vs. T3: SNF/0.1 PV

Figure 5 compares the fluid density profiles for test T2: S/0.1 PV with that of T3: SNF/0.1 PV. The corresponding x-z lateral views of CT scans as well as cross sectional CT slices are shown in Figure 6. The y-z lateral CT scans of tests T2 and T3 are also shown in Figure 7. The cross sectional CT slices during waterflooding of tests T2 and T3 are compared with each other at 0.4 PVI and 0.6 PVI, which are shown in Figure 6 (c) and Figure 7 (c), respectively. The blue regions in these figures represent the brine phase density, the red regions represent the solvent (a) or solvent based nanofluid (b) density, and the yellow regions represent the oil phase density.

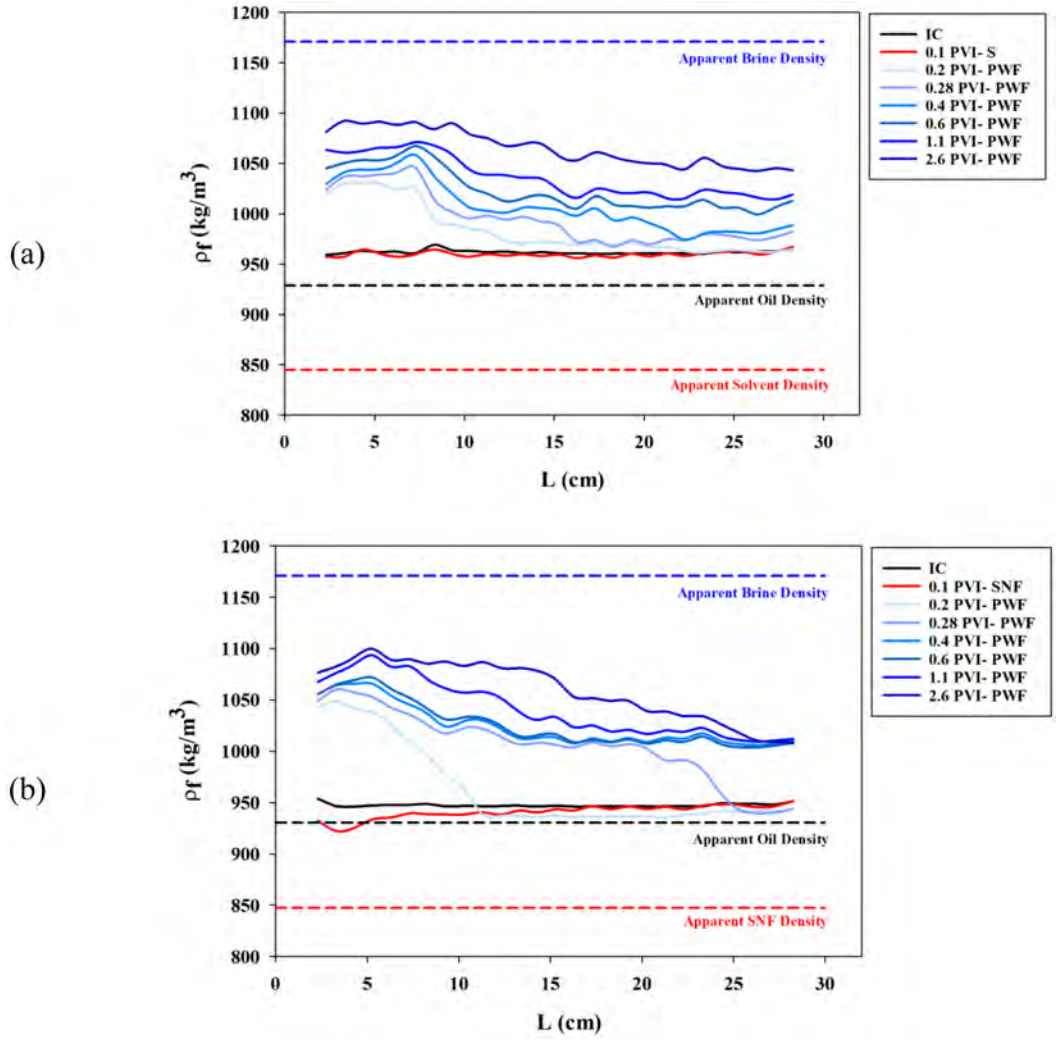

Figure 5—Fluid density profiles along the sandpack for tests (a) T2: S/0.1 PV, and (b) T3: SNF/0.1 PV at different pore volumes of injection. IC (black) is the initial condition (oil and water at connate water saturation). S, SNF, and PWF denote solvent (red in (a)), solvent based nanofluid (red in (b)), and post waterflooding (blue), respectively. Light to dark blue are profiles for post waterflooding as PVI increases.

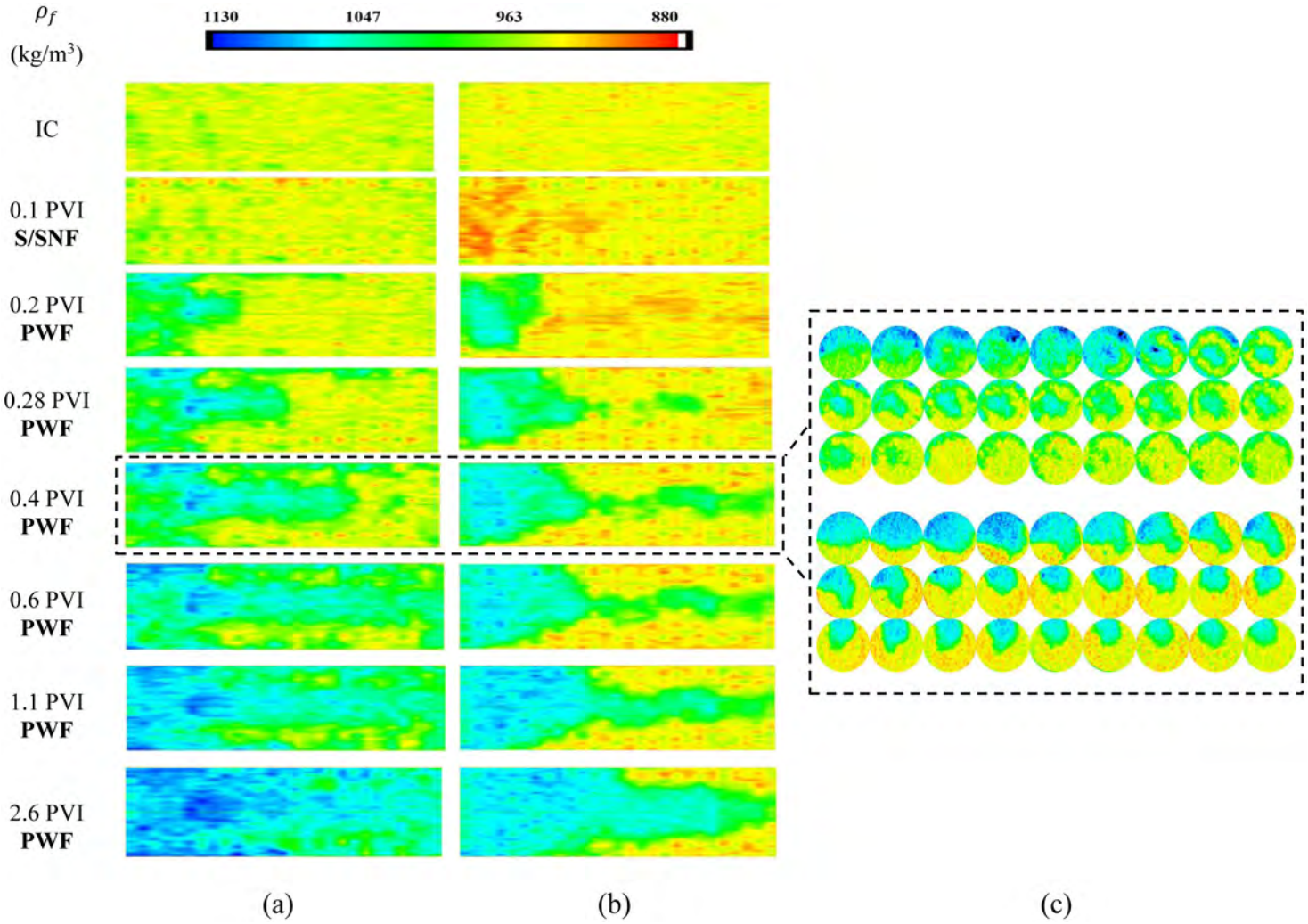

Figure 6—X-Z lateral CT scans during brine injection into an oil-saturated sandpack in the presence of (a) 0.1 PV solvent (T2) and (b) 0.1 PV solvent based nanofluid (T3). S, SNF, and PWF denote solvent, solvent based nanofluid, and post waterflooding, respectively. (c) Comparison of CT slices at 0.4 PVI for tests T2: S/0.1 PV and T3: SNF/0.1 PV. Each slice is 1 cm apart longitudinally.

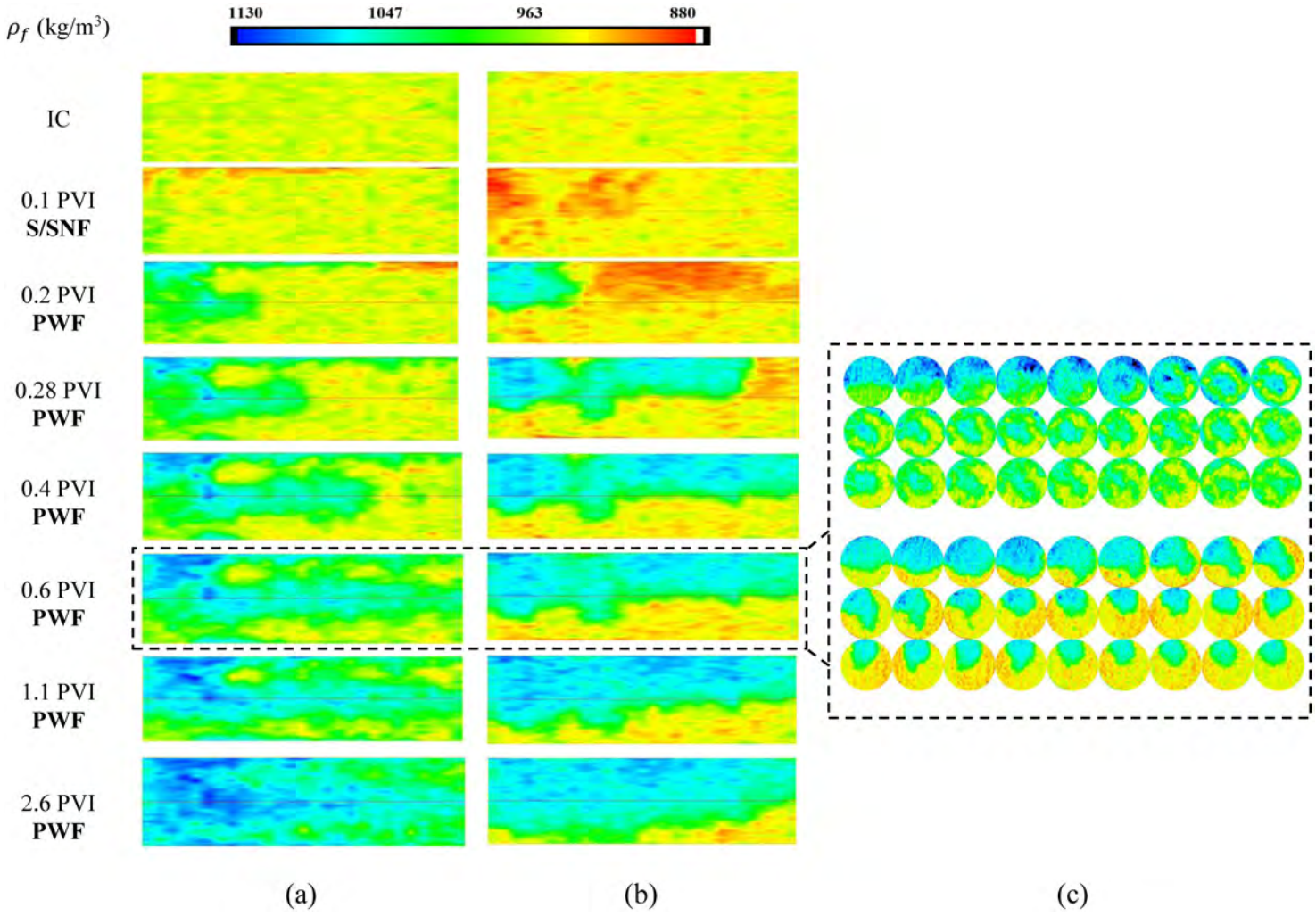

Figure 7—Y-Z lateral CT scans during brine injection into an oil-saturated sandpack in the presence of (a) 0.1 PV solvent (T2) and (b) 0.1 PV solvent based nanofluid (T3). Labels are as Figure 6. (c) Comparison of CT slices at 0.6 PVI for tests T2: S/0.1 PV and T3: SNF/0.1 PV. Each slice is 1 cm apart longitudinally. Gravity is downward in all images.

As it can be observed from Figure 5, the fluid density profiles are more uniform with later water breakthrough in the presence of solvent based nanofluid (T3) compared to the solvent alone (T2). Based on the x-z lateral CT scans in Figure 6, there are several water fingers on the walls and middle of the sandpack during waterflooding of test T2 in the presence of 0.1 pore volume solvent. However, several water fingers in test T2 are turned into one dominant finger in the core center in the presence of solvent based nanofluid (T3) especially after 0.4 pore volume of brine injection.

The vertical lateral view of the sandpack in the y-z plane shown in Figure 7 also reveals preferential water displacement in the presence of solvent based nanofluid (T3). Unlike test T2 where the chase water has swept the diluted oil randomly with several fingers, the water phase in test T3 has displaced all the regions that are invaded by solvent based nanofluid. Since the solvent phase tends to displace upper regions of the sandpack due to its lower density compared to the oil phase density (see Table 1), the water phase has also invaded the upper regions of the sandpack even though it naturally tends to have a gravity stable displacement. This clearly reveals that the presence of solvent based nanofluid is effective in re-distributing the flow paths of the water phase. The cross-sectional CT slices at 0.4 PVI and 0.6 PVI also reveal that during displacement of 0.1 pore volume of solvent by water (test T2), the water phase has invaded different areas of the sandpack and bypassed the oil phase in different regions. However, the displacement of 0.1 pore volume of solvent based nanofluid by water (test T3) is more preferential as the water phase invades

upper regions of the sandpack that are swept by the solvent based nanofluid. It seems that density contrast matters much more for the solvent based nanofluid, but not for the water. Additionally, the fluid density profiles in Figure 5 suggest a decrease in water phase mobility and better sweep of the regions invaded by solvent based nanofluid with water.

This is due to the in-situ emulsion formation at the interface of the invading brine and diluted oil due to the presence of partially hydrophobic silica NPs and a co-stabilizing surfactant in the solvent phase. As the brine phase invades the sandpack in the presence of solvent based nanofluid, the partially hydrophobic NPs and surfactant could preferably accumulate at the oil-water interface, resulting in the formation of in-situ emulsion via Roof snap-off at the pore scale [44–50]. The in-situ emulsions have higher viscosity compared to the invading brine, which prevent the water phase to create several fingers in the oil phase and stabilize the front in turn. The in-situ emulsion formation during waterflooding of solvent based nanofluid is resulted in local displacement efficiency improvement compared to the presence of solvent alone.

T4: S/1 PV vs. T5: SNF/1 PV. Figure 8 compares the fluid density profiles for test T4: S/1 PV with that of T5: SNF/1 PV. The corresponding x-z lateral views of CT scans as well as cross sectional CT slices are shown in Figure 9. Moreover, Figure 10 compares the y-z lateral CT scans during waterflooding of tests T4 and T5. Note that the only difference of tests T4 and T5 with tests T2 and T3 is in the solvent slug size, which has increased to 1 pore volume compared to that of 0.1 pore volume. The red regions in Figure 9 and Figure 10 represent the areas that are invaded either by solvent or solvent based nanofluid. Since solvent/ solvent based nanofluid have lower density than the oil phase, there is gravity override of solvent in the sandpack. That is why the red regions representing the solvent phase are in the upper regions of the sandpack in Figure 10.

Similar to the observations made at lower slug size, Figure 8 reveals a more uniform water displacement with later water breakthrough at larger solvent based nanofluid slug size compared to solvent alone. According to the vertical CT view in Figure 10 (b), as the brine phase invades the sandpack in the presence of solvent based nanofluid, it has displaced all the lower resistance regions displaced by solvent based nanofluid. That is why the water displacement shows some sign of gravity override especially before breakthrough time. After 1.5 PVI, water phase has expanded further and displaced some lower regions of the sandpack in a gravity stable form.

The water phase flow paths during displacement of 1 pore volume of either solvent or solvent based nanofluid can be also observed by comparing cross sectional CT slices in Figure 9 (c) and Figure 10 (c) at 1.18 PVI and 1.3 PVI. Both figures reveal that during displacement of 1 pore volume of solvent by water, the water phase has invaded different areas of the sandpack. However, the displacement of 1 pore volume of solvent based nanofluid by brine shows a completely different behavior where water has displaced upper areas of the sandpack uniformly and left the oil phase in lower regions of the sandpack.

The water displacement in the upper regions is primary due to greater dilution creating a lower viscosity oil phase there. As the brine phase invades the sandpack, the viscosity ratio (μ_D/μ_d) between the invading brine and diluted oil is smaller in the upper regions of the sandpack. Therefore, the brine phase preferably invades through the lower resistance paths in the upper regions compared to the lower ones. This is primary valid for both solvent and solvent based nanofluid cases. However, the water phase then invades downward for the solvent case but not for the solvent based nanofluid. For the solvent based nanofluid, water phase follows the solvent based nanofluid paths with a locally shock like front. This behavior is again related to in-situ emulsification between the brine and diluted oil, as can be observed by the sharp green interface shown by ovals and arrows in Figure 10 (b). This in-situ emulsification is related to the IFT reduction in the presence of surfactant and partially hydrophobic silica NPs as well as the shear present in porous media as a result of fluid flow. Both the shear rate and IFT reduction results in creation of emulsions at the interface of invading brine, resulting in a stabilized displacement front. The in-situ emulsions were also observed in the effluent. However, they were not stable and broke down after production.

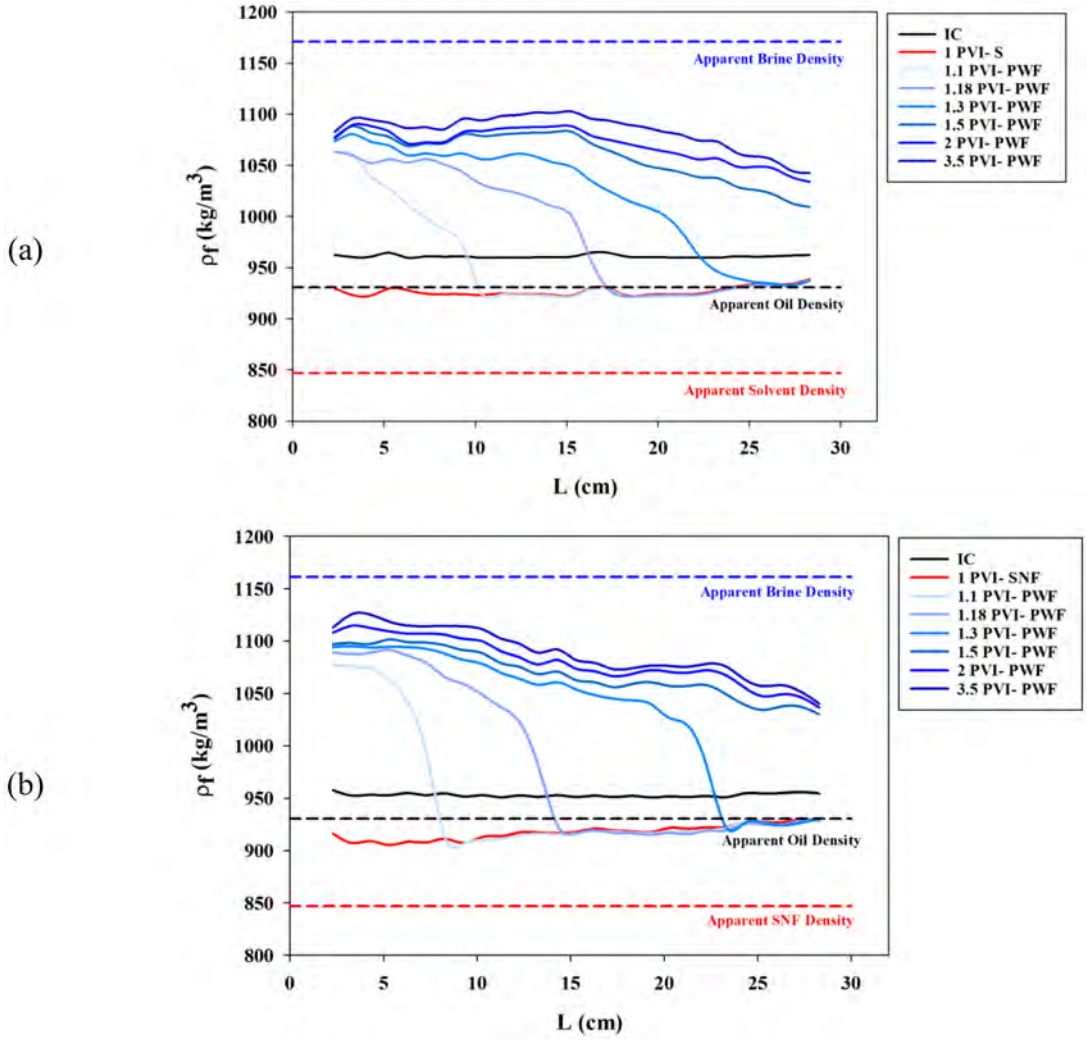

Figure 8—Fluid density profiles along the sandpack for tests (a) T4: S/1 PV, and (b) T5: SNF/1 PV at different pore volumes of injection. Colors and labels are as Figure 5.

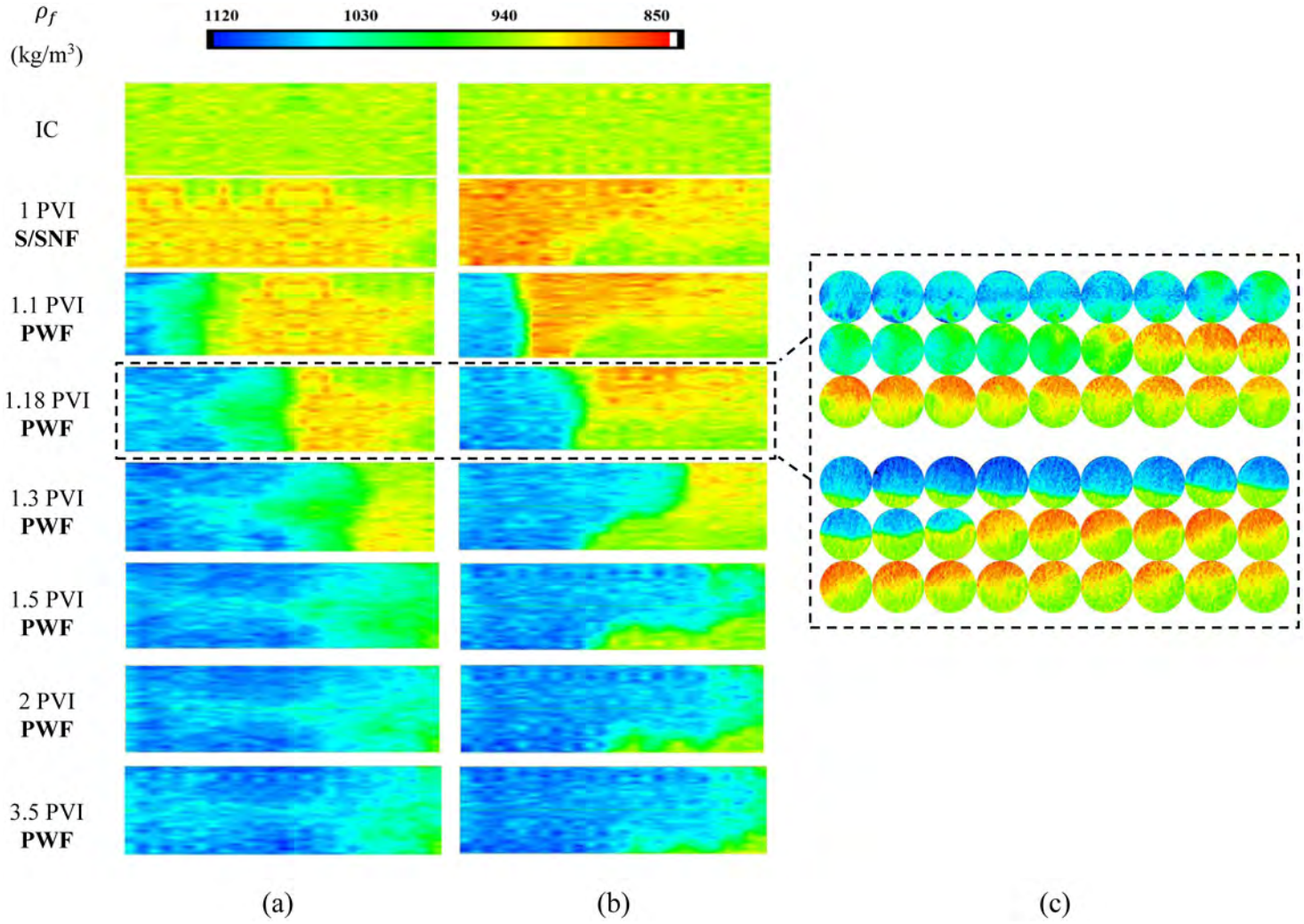

Figure 9—X-Z lateral CT scans during brine injection into an oil-saturated sandpack in the presence of (a) 1 PV solvent (T4) and (b) 1 PV solvent based nanofluid (T5). Labels are as Figure 6. (c) Comparison of CT slices at 1.18 PVI for tests T4: S/1PV and T5: SNF/1 PV. Each slice is 1 cm apart longitudinally.

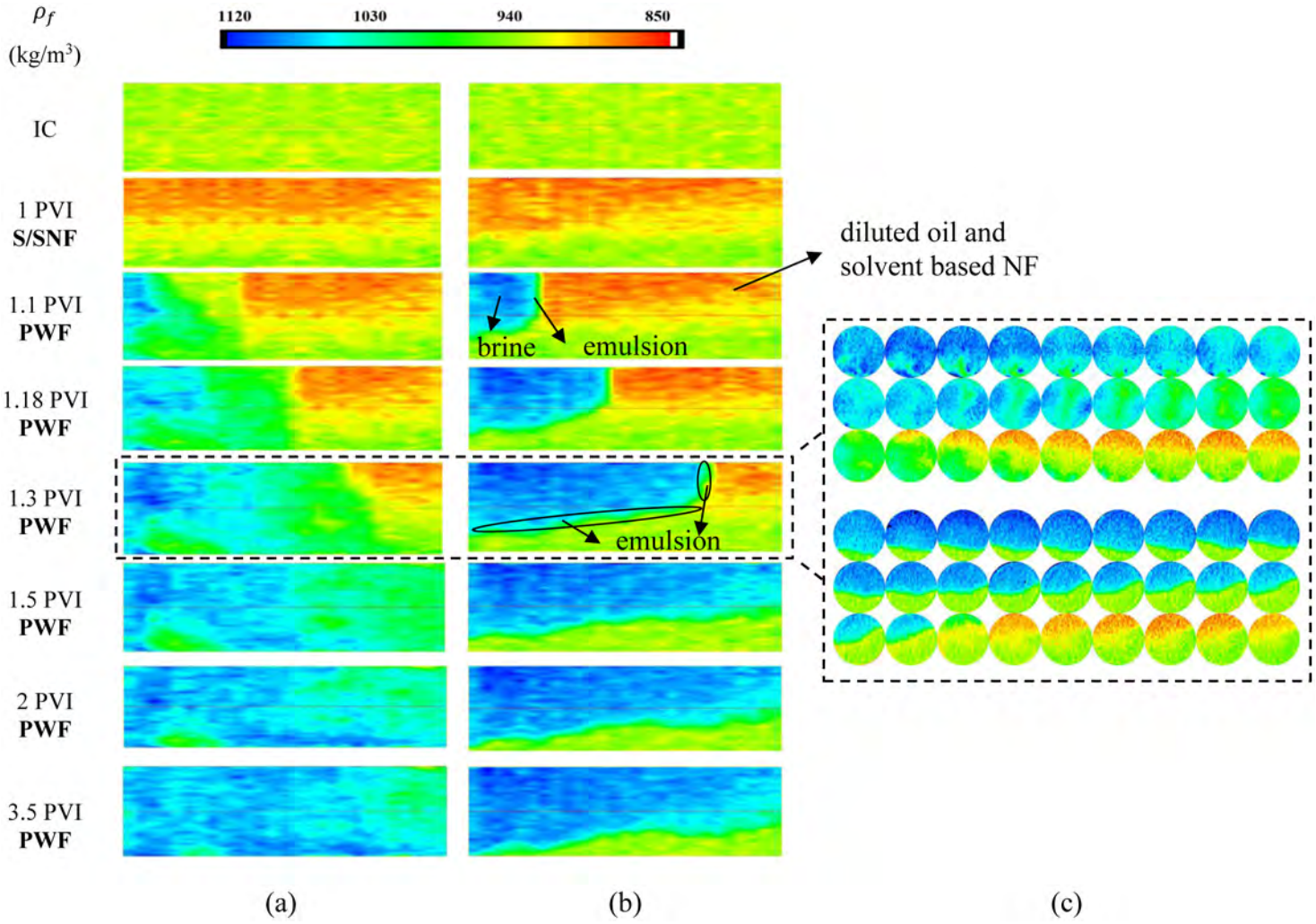

Figure 10—Y-Z lateral CT scans during brine injection into an oil-saturated sandpack in the presence of (a) 1 PV solvent (T4) and (b) 1 PV solvent based nanofluid (T5). Labels are as Figure 6. (c) Comparison of CT slices at 1.3 PVI for tests T4: S/1 PV and T5: SNF/1 PV. Each slice is 1 cm apart longitudinally. Gravity is downward in all images.

Although the in-situ emulsions at the water front are effective in preventing the brine phase from creating several fingers in the oil phase, the in-situ emulsions at the lower boundary of water tongue can prevent the water phase to sweep downward in a gravity stable form. Therefore, in addition to the viscosity ratio difference which retards the water phase invasion to the lower regions of the sandpack, the presence of in-situ emulsions at the lower boundary of water tongue can be another possible reason which prevents it from displacing the lower regions.

Upon post water flooding and water breakthrough, water entering the bottom half of the sand pack invades both into the swept zones and recovers the oil in the lower green zones. Therefore, the water phase is gradually displacing the lower regions of the sandpack at 3.5 PVI as shown in Figure 10 (b).

Although there are some signs of solvent gravity override at different solvent slug sizes of 0.1 and 1 pore volume, the presence of solvent based nanofluid at both slug sizes is effective in stabilizing the chase water displacement front and results in sweep efficiency improvement compared to the conventional solvent flooding.

Oil Recovery and Solvent Recovery Performances

Oil Recovery. Figure 11 shows the amount of oil recovered during injection of either solvent or solvent based nanofluid followed by water compared to the simple waterflooding. Table 5 also summarizes

important recovery results obtained during displacements of tests T1 to T5. The CT images at the end of post waterflooding for tests T1 to T5 are divided into half sections and analyzed to obtain residual oil saturation for the upper and lower half of the sandpack as shown in Table 5.

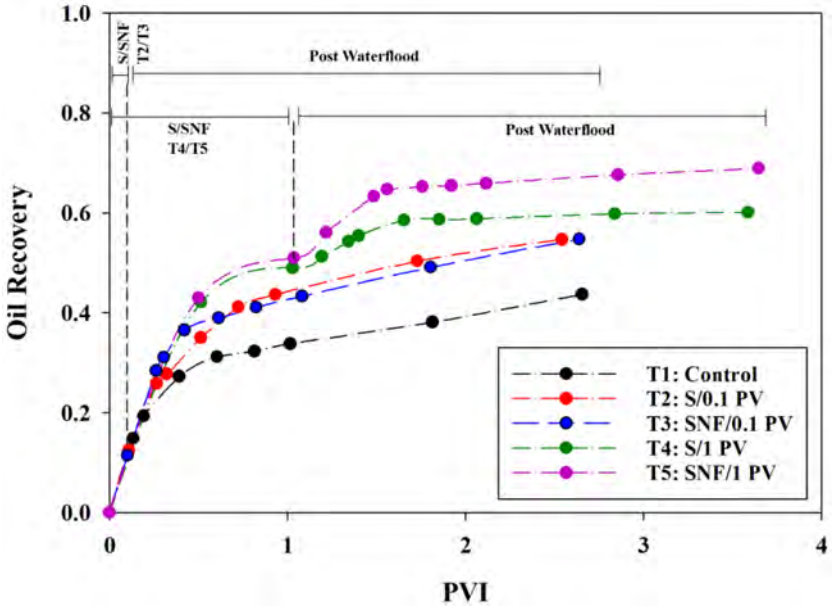

Figure 11—Oil recovery factor during solvent/solvent based nanofluid flooding followed by waterflooding for tests T1 to T5. S and SNF denote solvent and solvent based nanofluid, respectively.

According to Figure 11 and Table 5, the ultimate oil recovery during simple waterflooding in test T1 is about 44%. Furthermore, there is 8% lower residual oil saturation in the lower half of the sandpack (47%) compared to the upper half (55%). This suggests the water gravity underride during simple waterflooding as shown in Figure 4 (b). For tests T2 and T3, where respectively 0.1 pore volume of solvent and 0.1 pore volume of solvent based nanofluid are injected followed by water, the ultimate oil recovery values are the same and around 55%. Although the final oil recovery values of tests T2 and T3 are relatively the same, there is an improvement in the local displacement efficiency of test T3 as shown in Figure 6 and Figure 7. The improvement in local displacement efficiency is related to the dilute emulsion formation, which stabilizes the water displacement front. This stabilized front reduced the residual oil to 24% in the swept zones (see Table 5). However, the high bypassed oil saturation of 54% in the not-yet-swept zones (lower half of the sandpack) offset the small residual oil saturation of 24% in the swept zones (upper half of the sandpack). This resulted in the same amount of overall residual oil saturation of 39% for tests T2 and T3, even though the displacement profiles were different.

Unlike tests T2 and T3, the oil recovery factor during waterflooding of tests T4 and T5 with larger solvent slug sizes are different. According to Figure 11 and Table 5, the amount of oil recovery up to 1 pore volume is related to either solvent or solvent based nanofluid injection, which is about 50% for both T4 and T5 tests. After one pore volume, brine is injected to displace the diluted oil in the absence or presence of NPs and surfactant. As shown in Figure 11 and Table 5, the test T5 in the presence of solvent based nanofluid has 0.14 PVI later breakthrough time with around 9% higher final oil recovery compared to test T4. This is due to the more stable displacement of test T5 as a result of in-situ emulsification as shown in Figure 9 and Figure 10. Table 5 also reveals that the residual oil saturation in the swept zones (upper half of the sandpack) in test T5 is greatly reduced to 11%. However, it is 43% in the lower half of the sandpack which are not swept by the solvent based nanofluid. Although the displacement efficiency in test T5 was compromised by gravity override, the overall residual oil saturation (27%) was still 9% lower than that of T4 (36%). The presence of one pore volume of solvent based nanofluid was effective in stabilizing the chase water front,

which delayed the breakthrough time, reduced the residual oil in the swept zones substantially and resulted in higher oil recovery.

The comparison of tests T2 and T4 in Table 5 also reveals that as the solvent slug size is increased from 0.1 to 1 pore volume, the final oil recovery of waterflooding has increased by only 5%. Therefore, there is only 5% increase in the final oil recovery amount as the solvent slug size increases ten times. However, the comparison of tests T3 and T5 in Table 5 reveals that by increasing the solvent based nanofluid slug size from 0.1 to 1 pore volume, the final amount of oil recovery to waterflooding has increased by about 13%. This clearly reveals that increasing the solvent based nanofluid slug size has a more profound effect on the final oil production as it would be able to sustain the created emulsion for a longer period of time, resulting in more uniform displacement and higher oil recovery compared to smaller slug size.

Table 5—A summary of important recovery results for tests T1 to T5.

Test	T1: Control	T2: S/0.1 PV	T3: SNF/ 0.1 PV	T4: S/1 PV	T5: SNF/1 PV
PV at water BT	0.19	0.21	0.26	0.37	0.47
S_w at water BT	0.27	0.31	0.37	0.41	0.47
S_{or}	0.51	0.39	0.39	0.36	0.27
S_{or}, Upper half	0.55	0.39	0.24	0.38	0.11
S_{or}, Lower half	0.47	0.40	0.54	0.34	0.43
RF (%) at S/SNF flooding	N/A	12.4	11.4	49.1	50.9
RF (%) at WF/PWF	43.7	55.2	55.7	60.1	68.9
Solvent RF (%)	N/A	95.4	92.7	96.4	97.2

Solvent Recovery. As mentioned previously, due to the high solvent cost in solvent based processes, solvent retrieval is an important factor that needs to be considered in addition to the amount of oil recovery. Herein, the amount of solvent recovered during injection of either solvent or solvent based nanofluid followed by waterflooding is shown in Figure 12 for tests T2 to T5. According to Figure 12 and Table 5, the ultimate solvent recovery for tests T2 to T5 are more than 90% with the highest amount of solvent recovery for test T5 which is about 97%. This reveals that the chase water was able to recover most of the injected solvent for tests T2 to T5 with different solvent slug sizes.

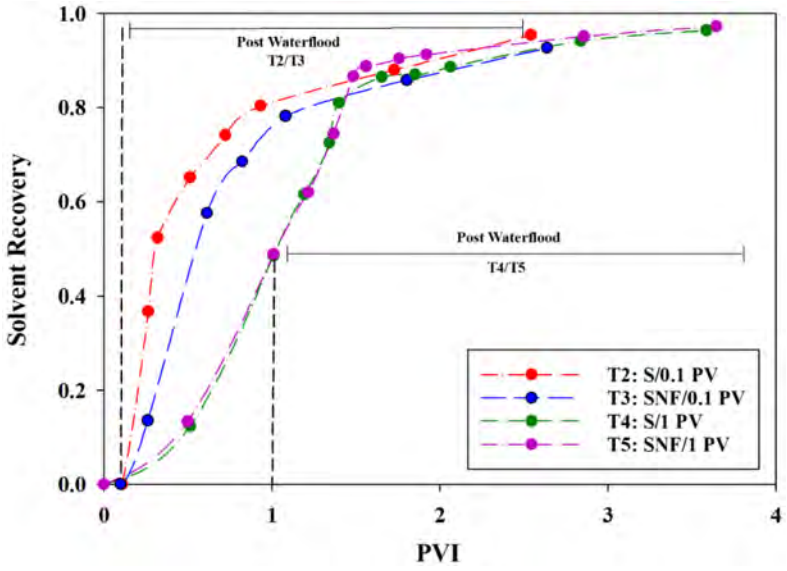

Figure 12—Solvent retrieval during solvent/solvent based nanofluid flooding followed by waterflooding for tests T2 to T5. S and SNF denote solvent and solvent based nanofluid, respectively.

Although solvent retrieval is more than 90% for tests T2 to T5, the efficiency of solvent based nanofluid flooding followed by waterflooding is still higher than conventional solvent flooding followed by waterflooding based on both fluid density profiles and oil recovery performances. To elaborate on, the combination of both oil recovery and solvent recovery results in Figure 11 and Figure 12 clearly reveal that solvent based nanofluid flooding followed by waterflooding is not only able to increase the sweep efficiency and oil recovery, but it is also effective in solvent retrieval. Although the solvent retrieval is relatively high in the case of conventional solvent flooding followed by waterflooding (see Table 5), the sweep efficiency improvement and oil recovery performance of conventional solvent flooding shown earlier are not as much significant as the solvent based nanofluid flooding. Therefore, the proposed technique can be both technically and economically feasible as it results in higher oil recovery and more uniform displacement compared to conventional solvent flooding followed by waterflooding and recovers significant amount of the solvent as well.

IFT and Contact Angle Analysis

Table 3 and Figure 13 show the interfacial tension (IFT) values between the oil and brine phases for tests T1 to T5 through the pendant drop method. In order to mimic the oil phases present in tests T2 to T5, the solvent and solvent based nanofluid were mixed with the oil phase in 1:10 volumetric ratio for tests T2 and T3, and in 1:1 volumetric ratio for tests T4 and T5. The interfacial tension between the prepared oil phases and brine (1 %wt. KI) were then measured using OCA 15EC instrument. It should be noted that brine (1 %wt. KI) was used as the surrounding phase for all cases and the prepared oil phases were injected from bottom to top for each case.

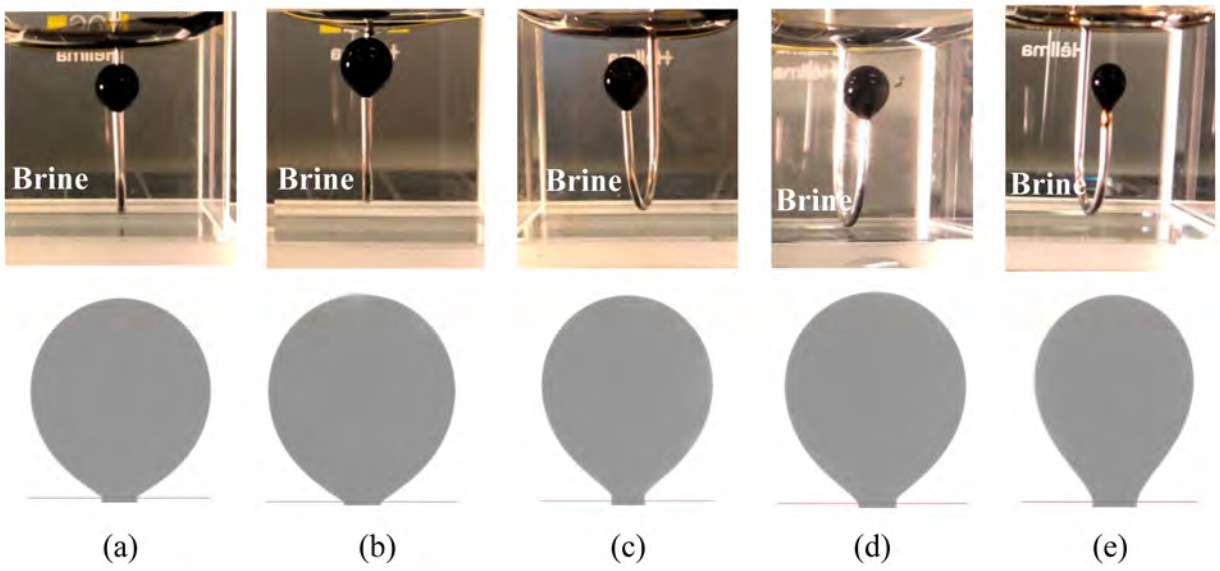

Figure 13—Shape of the oil droplets in the brine phase during IFT measurement for tests (a) T1: Control, (b) T2: S/0.1 PV, (c) T3: SNF/0.1 PV, (d) T4: S/1 PV and (e) T5: SNF/1 PV.

Table 3 and Figure 14 also reveal the results of contact angle measurement for tests T1 to T5. According to Figure 14, an oil droplet in the absence (T1) or presence of 1:1 volumetric ratio of solvent based nanofluid (T5) was placed on the Surfasil treated glass surface in the presence of brine (1 %wt. KI) as the surrounding phase. The contact angle values were then measured through the brine phase.

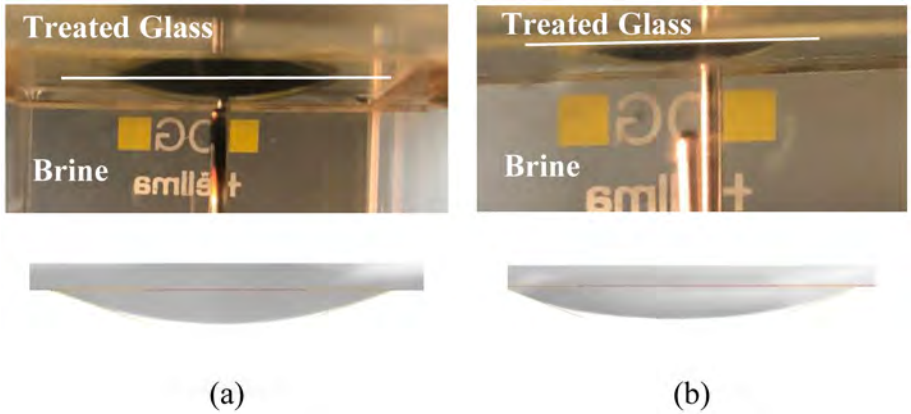

Figure 14—The oil droplets on the Surfasil treated glass surface in the presence of brine during contact angle measurement for tests (a) T1: control and (b) T5: SNF/1 PV.

Table 3—IFT and contact angle values for tests T1 to T5.

Test	T1: Control	T2: S/0.1 PV	T3: SNF/0.1 PV	T4: S/1 PV	T5: SNF/1 PV
IFT (mN/m)	23.1±0.1	23.4±0.5	18.7±0.2	23.6±0.1	7.8±0.1
Contact Angle (°)	159.1±0.6	N/A	N/A	N/A	159.9±0.5

According to Table 3 and Figure 13, the interfacial tension values are relatively close to each other for tests T1, T2, and T4. In other words, by increasing the solvent volume in the oil phase, the interfacial tension between the brine and oil phase has only slightly increased from 23.1±0.1 mN/m in test T1 to 23.4±0.5 mN/m in test T2 and 23.6±0.1 mN/m in test T4. Therefore, the IFT value does not change significantly as the

solvent slug size increases in the oil phase. The main improvements in oil recovery seen in Figure 11 for tests T2 and T4 are then related to the oil viscosity reduction in the presence of solvent.

For tests T3 and T5 on the other hand, the IFT values are respectively decreased to 18.7±0.2 mN/m and 7.8±0.1 mN/m compared to that of 23.1±0.1 mN/m for test T1. Therefore, there is a decrease in IFT value as the solvent based nanofluid slug size increases due to the presence of partially hydrophobic NPs and a surfactant in the solvent. The decrease in IFT value for test T3 is not significant compared to that of test T2 (19% reduction). This confirms that the local displacement efficiency improvement in test T3 compared to that of test T2 is related to the in-situ emulsification as discussed previously. Unlike test T3, there is a more pronounced IFT reduction for test T5 in the presence of 1:1 (v/v) solvent based nanofluid in the oil phase, which is 67% lower compared to that of test T4. The IFT reduction in test T5 has not only affected the final oil recovery as shown in Figure 11, but also provided the required energy to create a larger surface area through formation of emulsions at the brine invading front. The formation of in-situ emulsions in test T5 reduced water phase mobility and increased sweep efficiency as shown in Figure 10.

Unlike the IFT variation in the presence of solvent based nanofluid, the contact angle values are not changed significantly in the presence of solvent based nanofluid. According to the results in Table 3 and Figure 14, the contact angle value for test T1 is 159.1±0.6º, which is changed to 159.9±0.5º for test T5 with 1:1 (v/v) solvent based nanofluid. This suggests that there is no wettability alteration in the presence of solvent based nanofluid and that the wettability remains oil-wet even at the highest solvent based nanofluid slug size (T5). Therefore, the sweep efficiency and oil recovery observed in the presence of solvent based nanofluid cannot be related to the wettability alteration and are mainly affected by the oil viscosity reduction, IFT reduction, in-situ emulsification and the associated mobility control.

Pressure Drop Behavior

The pressure drop profiles during waterflooding of tests T1 to T5 are shown in Figure 15. It should be mentioned that the initial pressure drop in each test is the pressure drop during fluid flow at 0.5 cm^3/min prior to starting water injection. Therefore, the difference in the initial pressure drop for each test is related to the difference in the fluid flow condition prior to waterflooding. For example, the initial pressure drop for test T1 is the case where the oil phase is flowing at 0.5 cm^3/min in the sandpack. However, test T2 is the case where 0.1 pore volume of solvent as well as the oil phase are flowing at 0.5 cm^3/min. Since injecting the solvent in test T2 reduces the oil viscosity compared to test T1, the pressure drop decreases accordingly which can be observed in Figure 15. This can be also observed for test T4 where 1 pore volume of solvent as well as the oil phase are flowing at 0.5 cm^3/min. Since the oil viscosity decreases significantly in the presence of 1 pore volume of solvent, the initial pressure drop is even lower than that of test T2 with 0.1 pore volume of solvent. It should be mentioned that although the initial condition for tests T2 and T3 as well as tests T4 and T5 are the same, there are small differences in the initial pressure drop which is related to the differences in sandpack properties (see Table 2).

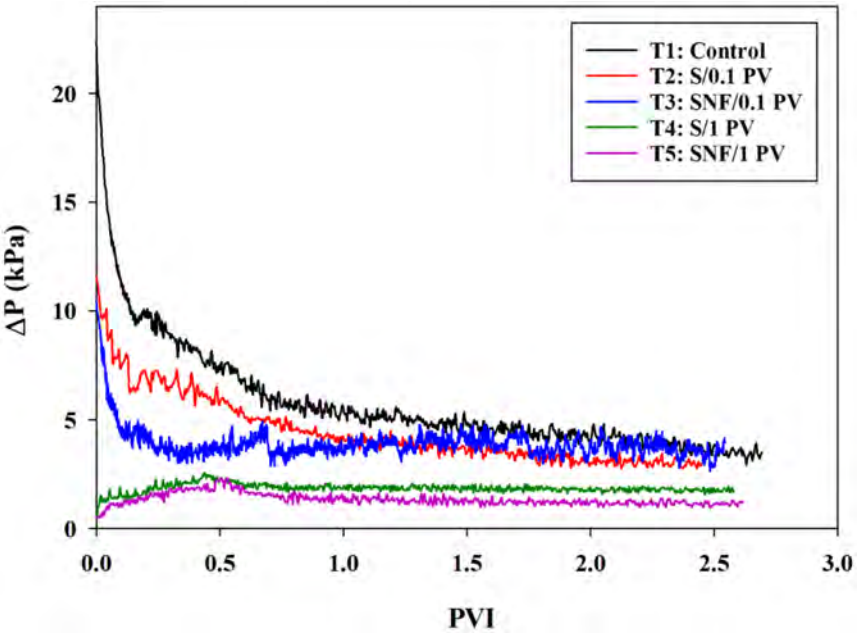

Figure 15—Pressure drop profiles during post waterflooding of tests T1 to T5. S and SNF represent solvent and solvent based nanofluid, respectively.

According to Figure 15, as the water phase invades the sandpack saturated with the oil phase in test T1, the water phase saturation increases and pressure drop decreases accordingly. The decreasing trend of pressure drop can be also observed in tests T2 and T3. Careful comparison of pressure drop profiles before 0.5 PVI for tests T2 and T3 shows that there is a sharp decrease in pressure drop for test T3 compared to that of test T2. This reveals that before 0.5 PVI, the oil production rate is higher for test T3 compared to that of test T2, which can be also observed in Figure 11. Therefore, the presence of 0.1 PV of solvent based nanofluid can suppress water fingering in comparison to 0.1 PV of solvent flooding (see Figure 7 (b)). This results in local displacement efficiency improvement in the presence of solvent based nanofluid, which accelerates the oil production rate accordingly. After 0.5 PVI, the pressure drop has a continuous decreasing trend for test T2, while there is a relatively constant trend for the test T3 with more pronounced fluctuations. The more pronounced pressure fluctuations in the test T3 would be related to the in-situ emulsion formation during waterflooding of 0.1 pore volume of solvent based nanofluid which has resulted in local displacement improvement and created a different pressure drop behavior compared to waterflooding of solvent alone.

The pressure drop profiles during waterflooding of tests T4 and T5 show an increasing and a decreasing trend which is different from previous cases. In both tests T4 and T5, the sandpack is firstly invaded by one pore volume of either solvent or solvent based nanofluid. As one pore volume of solvent or solvent based nanofluid is invaded to the sandpack, the oil phase becomes diluted gradually via miscible displacement. However, as water phase invades the sandpack afterwards, the displacement becomes immiscible, in which the relative permeability plays an important role on the flow performance. Since the pressure drop has an increasing trend during waterflooding of tests T4 and T5, it suggests that relative permeability for the brine phase upstream of the immiscible displacement front is small enough that its mobility is smaller than the mobility of the diluted oil phase. That is why the pressure drop increases before water breakthrough.

The pressure drop profiles also reveal that there is a delay in breakthrough time for test T5 compared to that of test T4. This is due to the more stable waterflooding of test T5 in the presence of solvent based nanofluid compared to that of test T4, as can be observed by fluid density profiles in Figure 10. Therefore, the pressure drop keeps its increasing trend for a longer time. After breakthrough, the pressure-drop decreases for both tests T4 and T5 as the water phase creates its percolating pathway in the porous media. The pressure drop then becomes relatively constant after 2 PVI for both cases. The lower magnitude of pressure drop

for test T5 is related to the higher oil production rate during waterflooding of test T5 as can be observed in Figure 11. Although the pressure drop value in test T5 is less than that of test T4, there is small difference between the values.

Unlike tests T2 and T3, the pressure-drop profiles during waterflooding of tests T4 and T5 with larger solvent slug size have the same trend and do not provide much information about the displacement efficiency. However, visual observations obtained from CT scanning along with the oil recovery and solvent recovery profiles in tests T4 and T5 provide a proper understanding of the efficiency of the proposed heavy oil recovery technique on sweep efficiency and oil recovery.

CONCLUSIONS

The effect of solvent based nanofluid flooding followed by waterflooding was investigated on sweep efficiency and oil recovery in an oil-wet porous media. The sweep efficiency improvement during such displacement was monitored with a CT scanner and compared to that of conventional solvent flooding followed by waterflooding. The following conclusions are made based on real time monitoring of density profiles, pressure drop as well as the oil and solvent recovery performances in the range of variables tested:

- Simple waterflooding of a medium viscosity heavy oil revealed both the fingered flow and gravitational segregation as a result of the adverse mobility ratio and density differences.
- Waterflooding of 0.1 pore volume of solvent based nanofluid revealed local displacement efficiency improvement compared to waterflooding of solvent alone due to the formation of emulsion at the invading brine interface. The local oil mobility enhancement in the presence of 0.1 PV of solvent based nanofluid accelerated the oil production rate, even though the ultimate oil recovery was the same as that of solvent alone.
- Waterflooding of one pore volume of solvent based nanofluid increased sweep efficiency and reduced the residual oil saturation to 11% in the swept zones. This was related to the formation of in-situ emulsion at the water-diluted oil interface which decreased the water phase mobility, suppressed water fingering, stabilized the displacement front, and resulted in 9% higher oil recovery compared to waterflooding of solvent alone.
- Increasing the solvent based nanofluid slug size to ten times had a more profound effect on oil recovery than increasing the solvent slug size. This was due to the in-situ emulsion formation in the presence of solvent based nanofluids as well as the ability of the generated emulsions to sustain through the porous media at larger solvent based nanofluid slug size.
- Increasing the solvent slug size had a slight effect on IFT variation. However, there were a decrease of about 19% and 67% as the solvent based nanofluid slug size increased ten times. This IFT reduction promoted the emulsification and resulted in displacement efficiency improvement in the presence of solvent based nanofluid.
- The chase water in either solvent or solvent based nanofluid retrieved more than 90% of the solvent at different slug sizes of 0.1 PV and 1 PV, making the technique economically viable.
- Although some sign of solvent gravity override was observed in both solvent injection and solvent based nanofluid injection, the chase water swept the solvent based nanofluid paths uniformly and yielded a significant decrease in the residual oil saturation in the swept zones. Thus, the overall displacement efficiency would be even more desirable in the absence of solvent gravity override.

ACKNOWLEDGEMENTS

This research was undertaken, in part, thanks to funding from the Canada Excellence Research Chair program in Materials Engineering for Unconventional Reservoirs (CERC).

NOMENCLATURE

BT	breakthrough time
CSI	cyclic solvent injection
CSS	cyclic steam stimulation
CT	computed tomography
ES-SAGD	expanding solvent-steam assisted gravity drainage
HMDS	hexamethyldisilazane
HSNP	partially hydrophobic silica nanoparticle
LASER	liquid addition to steam to enhance recovery
NF	nanofluid
NPs	Nanoparticles
PV	pore volume (cm^3)
PVI	pore volume injected (cm^3)
PWF	post waterflooding
RF	recovery factor
RPM	revolutions per minute (min^{-1})
S	solvent
SAGD	steam-assisted gravity drainage
SNF	solvent based nanofluid
s/w	solvent in water
WF	waterflooding

Symbols

d	Darcy
k	permeability
Q	volumetric flow rate (cm^3/min)
S_{oi}	initial oil saturation
S_{or}	residual oil saturation
S_w	water saturation
S_{wi}	initial water saturation
ρ	density (kg/m^3)
$\boldsymbol{\rho_f}$	fluid density (kg/m^3)
μ	viscosity (mPas)
μ_D	displaced phase viscosity (mPas)
μ_d	dispacling phase viscosity (mPas)
V	velocity (m/s)
x	Cartesian coordinate
y	Cartesian coordinate
z	Cartesian coordinate

Subscripts

o	oil
s	solvent
w	water

REFERENCES

1. Kumar, R.; Dao, E. K.; Mohanty, K. K. In *Emulsion flooding of heavy oil*, SPE Improved Oil Recovery Symposium, Society of Petroleum Engineers: 2010.
2. Fu, X. Enhanced oil recovery of viscous oil by injection of water-in-oil emulsion made with used engine oil. 2012.
3. Ali, S. In *Non-thermal heavy oil recovery methods*, SPE Rocky Mountain Regional Meeting, Society of Petroleum Engineers: 1976.
4. Liu, Q.; Dong, M.; Ma, S. In *Alkaline/surfactant flood potential in Western Canadian heavy oil reservoirs*, SPE/DOE Symposium on Improved Oil Recovery, Society of Petroleum Engineers: 2006.
5. Mohsenzadeh, A.; Al-Wahaibi, Y.; Jibril, A.; Al-Hajri, R.; Shuwa, S., The novel use of deep eutectic solvents for enhancing heavy oil recovery. *Journal of Petroleum Science and Engineering* 2015, **130**, 6–15.
6. Wu, Y.; Mahmoudkhani, A.; Watson, P.; Fenderson, T.; Kolla, H. S.; Nair, M. In *A non-thermal surfactant-polymer based technology for enhanced heavy oil recovery in oil sand and ultra shallow reservoirs*, SPE Heavy Oil Conference Canada, Society of Petroleum Engineers: 2012.
7. Babadagli, T.; Cao, N., Can water-alternating-solvent injection be an option for efficient heavy-oil recovery?: An experimental analysis for different reservoir conditions. *Journal of Petroleum Science and Engineering* 2018, **170**, 485–496.
8. Dehghan, A.; Farzaneh, S.; Kharrat, R.; Ghazanfari, M.; Rashtchian, D., Pore-level investigation of heavy oil recovery during water alternating solvent injection process. *Transport in Porous Media* 2010, **83** (3), 653–666.
9. StalkupF. I.,Jr, Miscible Displacement, volume 8 of SPE Monograph Series. *Society of Petroleum Engineers, Dallas, TX* **1983**.
10. Allen, J. C.; Woodward, C. D.; Brown, A.; Wu, C. H., Multiple solvent heavy oil recovery method. *Google Patents*: 1976.
11. Lim, G. B.; Kry, P. R.; Lebel, J. P.; Kwan, M. Y., Cyclic solvent process for in-situ bitumen and heavy oil production. *Google Patents*: 2004.
12. Baker, L., Effects of dispersion and dead-end pore volume in miscible flooding. *Society of Petroleum Engineers Journal* 1977, **17** (03), 219–227.
13. Butler, R. M.; Mokrys, I. J., A new process (VAPEX) for recovering heavy oils using hot water and hydrocarbon vapour. *Journal of Canadian Petroleum Technology* 1991, **30** (01).
14. Cui, J.; Babadagli, T., Retrieval of solvent injected during heavy-oil recovery: Pore scale micromodel experiments at variable temperature conditions. *International Journal of Heat and Mass Transfer* 2017, **112**, 837–849.
15. Ali, S.; Abad, B., Bitumen recovery from oil sands, using solvents in conjunction with steam. *Journal of Canadian Petroleum Technology* 1976, **15** (03).
16. Nasr, T.; Beaulieu, G.; Golbeck, H.; Heck, G., Novel expanding solvent-SAGD process" ES-SAGD". *Journal of Canadian Petroleum Technology* 2003, **42** (01).
17. Nasr, T.; Ayodele, O., Thermal Techniques for the Recovery of Heavy Oil and Bitumen. Paper SPE 97488 presented at SPE International Improved Oil Recovery Conference in Asia Pacific, Kuala Lumpur, Malaysia, 5–6 December. 2005.
18. Nasr, T. N.; Ayodele, O. R. In *New hybrid steam-solvent processes for the recovery of heavy oil and bitumen*, Abu Dhabi International Petroleum Exhibition and Conference, Society of Petroleum Engineers: 2006.
19. Redford, D. A.; McKay, A. S. In *Hydrocarbon-steam processes for recovery of bitumen from oil sands*, SPE/DOE Enhanced Oil Recovery Symposium, Society of Petroleum Engineers: 1980.

20. Shu, W.; Hartman, K., Effect of solvent on steam recovery of heavy oil. *SPE reservoir Engineering* 1988, **3** (02), 457–465.
21. Zhao, L.; Nasr, T.; Huang, H.; Beaulieu, G.; Heck, G.; Golbeck, H., Steam alternating solvent process: lab test and simulation. *Journal of Canadian Petroleum Technology* 2005, **44** (09).
22. Huang, S.; Chen, X.; Liu, H.; Jiang, J.; Cao, M.; Xia, Y., Experimental and numerical study of solvent optimization during horizontal-well solvent-enhanced steam flooding in thin heavy-oil reservoirs. *Fuel* 2018, **228**, 379–389.
23. Faradonbeh, M.; Harding, T. G.; Abedi, J., Semianalytical modeling of steam/solvent gravity drainage of heavy oil and bitumen: unsteady-state model with curved interface. *SPE Reservoir Evaluation & Engineering* 2017, **20** (01), 134–148.
24. Butler, R. M.; Mokrys, I. J., Recovery of heavy oils using vapourized hydrocarbon solvents: further development of the VAPEX process. *Journal of Canadian Petroleum Technology* 1993, **32** (06).
25. Ivory, J.; Zheng, R.; Nasr, T.; Deng, X.; Beaulieu, G.; Heck, G., Investigation of low pressure ES-SAGD. Paper SPE 117759 presented at the International Thermal Operations and Heavy Oil Symposium, Calgary, Alberta, Canada. October: 2008.
26. Pathak, V.; Babadagli, T.; Edmunds, N. R. In *Hot solvent injection for heavy oil/bitumen recovery: an experimental investigation*, Canadian Unconventional Resources and International Petroleum Conference, Society of Petroleum Engineers: 2010.
27. Pathak, V.; Babadagli, T.; Edmunds, N., Heavy oil and bitumen recovery by hot solvent injection. *Journal of petroleum science and engineering* 2011, **78** (3-4), 637–645.
28. Frauenfeld, T. W.; Jossy, C.; Ivory, J., Numerical simulation and economic evaluation of hybrid solvent processes. *Journal of Canadian Petroleum Technology* 2010, **49** (07), 28–35.
29. Deng, X.; Huang, H.; Zhao, L.; Law, D.-S.; Nasr, T., Simulating the ES-SAGD process with solvent mixture in Athabasca reservoirs. *Journal of Canadian Petroleum Technology* 2010, **49** (01), 38–46.
30. Ardali, M.; Barrufet, M. A.; Mamora, D. D.; Qiu, F. In *A critical review of hybrid steam/solvent processes for the recovery of heavy oil and bitumen*, SPE Annual Technical Conference and Exhibition, Society of Petroleum Engineers: 2012.
31. Zhang, K.; Zhou, X.; Peng, X.; Zeng, F., A comparison study between N-Solv method and cyclic hot solvent injection (CHSI) method. *Journal of Petroleum Science and Engineering* 2019, **173**, 258–268.
32. Leyva-Gomez, H.; Babadagli, T., Efficiency of heavy-oil/bitumen recovery from fractured carbonates by hot-solvent injection. *Journal of Petroleum Science and Engineering* 2018, **165**, 752–764.
33. Jha, K., A laboratory study of heavy oil recovery with carbon dioxide. *Journal of Canadian Petroleum Technology* 1986, **25** (02).
34. Teklu, T. W.; Alameri, W.; Kazemi, H.; Graves, R. M. In *Contact angle measurements on conventional and unconventional reservoir cores*, Unconventional Resources Technology Conference (URTEC): 2015.
35. Shokri, A. R.; Babadagli, T., Field scale modeling of CHOPS and solvent/thermal based post CHOPS EOR applications considering non-equilibrium foamy oil behavior and realistic representation of wormholes. *Journal of Petroleum Science and Engineering* 2016, **137**, 144–156.
36. Rangriz Shokri, A.; Babadagli, T., A sensitivity analysis of cyclic solvent stimulation for Post-CHOPS EOR: application on an actual field case. *SPE Economics & Management* 2016, **8** (04), 78–89.

37. Rangriz Shokri, A.; Babadagli, T., Laboratory measurements and numerical simulation of cyclic solvent stimulation with a thermally aided solvent retrieval phase in the presence of wormholes after cold heavy oil production with sand. *Energy & Fuels* 2016, **30** (11), 9181–9192.
38. Christie, M.; Bond, D., Detailed simulation of unstable processes in miscible flooding. *SPE Reservoir Engineering* 1987, **2** (04), 514–522.
39. Tchelepi, H.; OrrF.,Jr, Interaction of viscous fingering, permeability heterogeneity, and gravity segregation in three dimensions. *SPE Reservoir Engineering* 1994, **9** (04), 266–271.
40. Batruny, P.; Babadagli, T., Effect of waterflooding history on the efficiency of fully miscible tertiary solvent injection and optimal design of water-alternating-gas process. *Journal of Petroleum Science and Engineering* 2015, **130**, 114–122.
41. Sarma, H.; Maini, B.; Jha, K., Evaluation of emulsified solvent flooding for heavy oil recovery. *Journal of Canadian Petroleum Technology* 1998, **37** (07).
42. Kumar, G.; Kakati, A.; Mani, E.; Sangwai, J. S. In *Nanoparticle Stabilized Solvent-Based Emulsion for Enhanced Heavy Oil Recovery*, SPE Canada Heavy Oil Technical Conference, Society of Petroleum Engineers: 2018.
43. Maaref, S.; Kantzas, A.; Bryant, S. L., The effect of silanization assisted nanoparticle hydrophobicity on emulsion stability through droplet size distribution analysis. *Chemical Engineering Science* 2019, **201**, 175–190.
44. Maaref, S.; Kantzas, A.; Bryant, S., Investigating sweep efficiency improvement in oil-wet porous media by the application of functionalized nanoparticles. *Fuel* 2020, **267**, 117263.
45. Maaref, S.; Kantzas, A.; Bryant, S. L., The effect of water alternating solvent based nanofluid flooding on heavy oil recovery in oil-wet porous media. *Fuel* 2020, **282**, 118808.
46. Aminzadeh-goharrizi, B.; DiCarlo, D. A.; Hyun Chung, D.; Roberts, M.; Bryant, S. L.; Huh, C. In *Effect of spontaneous formation of nanoparticle stabilized emulsion on the stability of a displacement*, SPE Improved Oil Recovery Symposium, Society of Petroleum Engineers: 2012.
47. Aminzadeh-Goharrizi, B.; DiCarlo, D. A.; Chung, D.; Kianinejad, A.; Bryant, S. L.; Huh, C. In *Effect of nanoparticles on flow alteration during CO 2 injection*, SPE Annual Technical Conference and Exhibition, Society of Petroleum Engineers: 2012.
48. Aminzadeh, B.; Chung, D.; Zhang, X.; Bryant, S. L.; Huh, C.; DiCarlo, D. In *Influence of surface-treated nanoparticles on displacement patterns during CO injection*, SPE annual technical conference and exhibition, Society of Petroleum Engineers: 2013.
49. Chung, D. H., Transport of nanoparticles during drainage and imbibition displacements in porous media. **2013**.
50. Wung, R. M. Utilizing surface treated nanoparticles for enhanced geologic carbon sequestration. 2015.